united nations
educational, scientific
and cultural
organization

international atomic
energy agency

the
abdus salam
international centre for theoretical physics

SMR/1270-15

SCHOOL ON SYNCHROTRON RADIATION

6 November - 8 December 2000

Miramare - Trieste, Italy

Supported in part by the Italian Ministry of Foreign Affairs in connection with the SESEME project

Co-sponsors: Sincrotrone Trieste, Società Italiana di Luce di Sincrotrone (SILS) and the Arab Fund for Economic and Social Development

Small Angle X-ray Scattering (SAXS)

by Heterogeneous Materials

A. Craievich
Universidade de Sao Paulo
Brazil

INTERNATIONAL ATOMIC ENERGY AGENCY
UNITED NATIONS EDUCATIONAL, SCIENTIFIC AND CULTURAL ORGANIZATION
INTERNATIONAL CENTRE FOR THEORETICAL PHYSICS
I.C.T.P., P.O. BOX 586, 34100 TRIESTE, ITALY, CABLE: CENTRATOM TRIESTE

UNITED NATIONS INDUSTRIAL DEVELOPMENT ORGANIZATION

INTERNATIONAL CENTRE FOR SCIENCE AND HIGH TECHNOLOGY
c/o INTERNATIONAL CENTRE FOR THEORETICAL PHYSICS 34100 TRIESTE (ITALY) VIA GRIGNANO, 9 (ADRIATICO PALACE) P.O. BOX 586 TELEPHONE 040 224572 TELEFAX 040 224575 TELEX 460449 APH I

H4.SMR/676-28

SECOND SCHOOL ON THE USE OF SYNCHROTRON RADIATION IN SCIENCE AND TECHNOLOGY: *"JOHN FUGGLE MEMORIAL"*

25 October - 19 November 1993

Miramare - Trieste, Italy

Small Angle X-ray Scattering (SAXS) by

Heterogeneous Materials

A. Craievich
National Laboratory for Synchrotron Radiation
(LNLS)
Campinas, Brazil

III) Small γ Scattering (SAXS) by heterogeneous materials

- Basic theory
- Guinier's Law. Porod's Law. Invariant
- Crystalization in glasses
- Aggregation and gelation (fractal structures)
- Phase-separation in glasses
- Application of anomalous scattering
- SAXS instrumentation

SAXS

General case:

$$A(\vec{q}) = A_e \int \rho(\vec{r})\, e^{-i\vec{q}\vec{r}}\, d\vec{r}$$

$$\rho(\vec{r}) = \int \frac{A(s)}{A_e}\, e^{i\vec{q}\vec{r}}\, d\vec{q}$$

$$I(\vec{s}) = |A(\vec{s})|^2 = A_e^2 \left| \int \rho(\vec{r})\, e^{-i\vec{q}\vec{r}}\, d\vec{r} \right|^2$$

$$(= AA^*)$$

$$I(\vec{q}) = \int\int \rho(\vec{u}')\, \rho(\vec{u})\, e^{-i\vec{q}(u'-u)}\, du'\, du$$

$$\vec{u}' - \vec{u} = \vec{r} \therefore \vec{u}' = \vec{u} + \vec{r}$$

$$I(\vec{q}) = \int\int \rho(u + \vec{r})\, \rho(\vec{u})\, e^{-i\vec{q}\vec{r}}\, d\vec{r}\, du$$

$$= \int \underbrace{\left[\int \rho(\vec{u} + \vec{r})\, \rho(\vec{u})\, d\vec{u}\right]}_{P(\vec{r})} e^{-i\vec{q}\vec{r}}\, dr$$

$$I(\vec{q}) = \int P(\vec{r})\, e^{-i\vec{q}\vec{r}}\, d\vec{r}$$

$$P(\vec{r}) = \int I(\vec{q})\, e^{i\vec{q}\vec{r}}\, d\vec{q}$$

Princípio de Babinet

$$A(q) = \int \rho(\vec{r})\, e^{-i\vec{q}\vec{r}}\, d\vec{r}$$

$$A(q) = \int \left[\rho_o + n(\vec{r})\right] e^{-i\vec{q}\vec{r}}\, d\vec{r}$$

$$= \int \underbrace{\rho_o\, e^{-i\vec{q}\vec{r}}\, d\vec{r}}_{\| \; 0} + \int n(\vec{r})\, e^{-i\vec{q}\vec{r}}\, d\vec{r}$$

$$I(\vec{q}) = \int \left[n(\vec{u})\, n(\vec{u} + \vec{r})\, d\vec{u}\right] e^{-i\vec{q}\vec{r}}\, d\vec{r}$$

For q -> 0

$$I(0) = v\,\overline{n^2}$$

Defining:

$$\gamma(\vec{r}) = \frac{1}{v\,\overline{n^2}} \int n(u)\, n(u+\vec{r})\, d\vec{u}$$

$$\rightarrow I(\vec{q}) = \overline{n^2}\, v \int \gamma(\vec{r})\, e^{-i\vec{q}\vec{r}}\, d\vec{r}$$

For isotropic systems:

$$I(q) = \overline{n^2}\, v \int \gamma(r) \frac{\sin qr}{qr} 4\pi r^2\, dr$$

Assymptotic behaviors:

a) q -> 0 (Guinier's law)

$$I(q) = I(0)\, e^{-}$$ otropic systems)

$$I(\vec{q}) = I(0)\, e^{-(\vec{q}.\vec{R}_D)^2}$$

$$R_D^2 = \frac{\int r_D^2\, \rho(\vec{r})\, d\vec{r}}{\int \rho(\vec{r})\, d\vec{r}}$$

b) q -> 0

$$I(0) = N\, n^2 = N(\rho - \rho_o)^2\, v^2$$

General case:

$$I(0) = n^2\, \overline{N} \frac{kT}{v} \beta\,; \beta = -\frac{1}{V}\left(\frac{\partial V}{dP}\right)_T$$

c) q -> 0 (Porod's law)

$$I(q) = 2\pi(n - n_o)^2 \frac{S}{q^4}$$ (leading term)

$$I(q) = \frac{A}{q^4} + \frac{B}{q^6} + \ldots +$$

(include oscillation contribution)

$$+ \frac{f_1(u_1 q)\cos u}{h^3} + \frac{f_2(u_1 q)\sin u}{h^3} ; u = qR_1 \quad .$$

Integral parameters

$$\int q^2 \, I(q)\, dq = 2\pi^2 \;\; Nn^2 \, v$$ (dilute system)

$$\int q^2 \, I(q)\, dq = 2\pi^2 \, n^2 V \, c(1-c)$$

c: volume fraction

V: irradiated volume

N: number of particles per unit volume

υ: particle volume

$$\ell_c = \frac{2}{4\pi \, V \, n^2 \, c(1-c)} \int_o^\infty q \, I(q)\, dq$$

Dense system of identical particles:

I(h) = ϕ P(q) S(q)

$$A(\vec{q}) = \sum_k \left[\sum_\ell f_{k\ell} \, e^{-iq(\vec{R}_k + \vec{r}_{k\ell})} \right]$$

For particles with center of simmetry:

$$A(\vec{q}) = \sum_k e^{-i\vec{q}\vec{r}} \sum_\ell f_{k\ell} \cos(\vec{q}\vec{r}_{k\ell})$$

$$I(q) = \Phi\, P(q)\, S(q)$$

$$q = \frac{4\pi}{\lambda} \sin \varepsilon/2$$

$$P(q) = V^2 (\rho - \rho_\circ)^2 \left[3\sin(qr_\circ) - qr_\circ \cos(qr_\circ) / (qr_\circ)^3 \right]^2$$

$$P(q) = 2\pi (\rho - \rho_\circ)\, S / q^4$$

$$q \to \infty$$

Guinier: $$\frac{P = P(0)\, e^{-R_G^2 q^2/3}}{q \to 0}$$

Porod: $$\frac{P = K\, S / q^4}{q \to \infty}$$

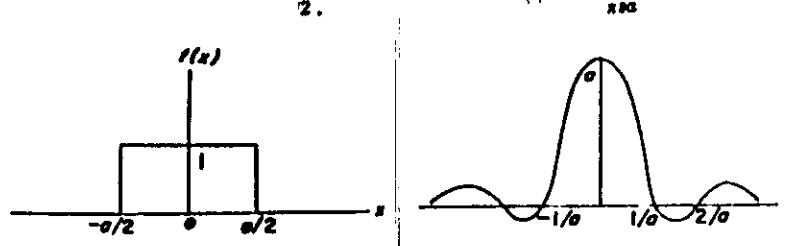

10. Triangular function:

$f(x) \begin{cases} = a\left(1 - \frac{|x|}{a}\right) & \text{for } |x| < a, \\ = 0 & \text{for } |x| > a. \end{cases}$

$F(s) = a^2 \frac{\sin^2 \pi a s}{(\pi a s)^2}$

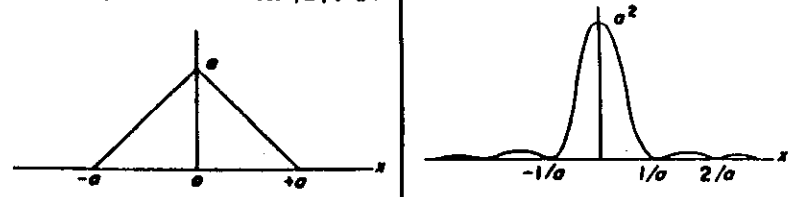

11. Exponential function:

$f(x) = \exp(-\gamma |x|)$

$F(s) = \frac{2\gamma}{\gamma^2 + (2\pi s)^2}$ (Cauchy function)

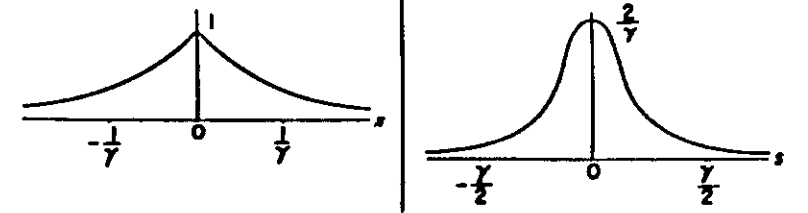

12. Form factor of a sphere:

$f(x) \begin{cases} = 1 & \text{for } |x| < R, \\ = 0 & \text{for } |x| > R. \end{cases}$

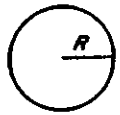

$F(s)$ has spherical symmetry

$F(s) = \frac{4}{3}\pi R^3 \Phi(2\pi s R)$,

with $\Phi(u) = 3\frac{(\sin u - u \cos u)}{u^3}$

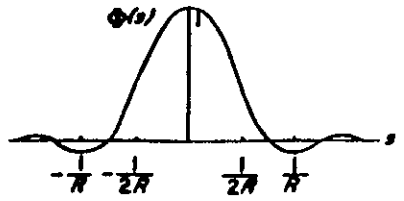

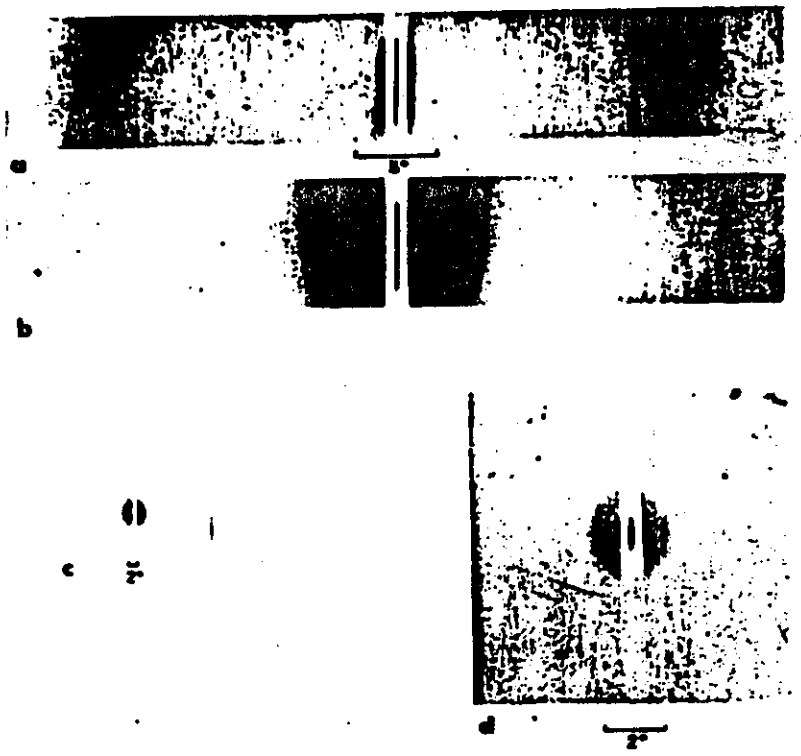

SAXS

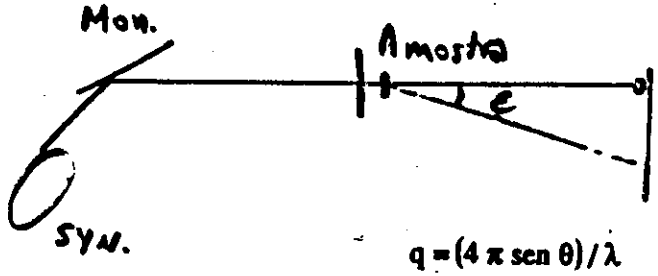

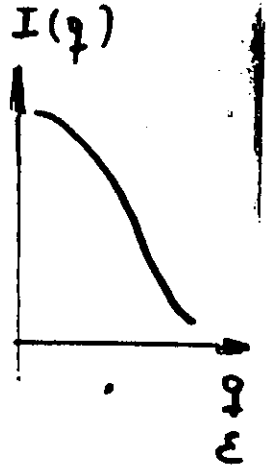

$$q = (4\pi \operatorname{sen}\theta)/\lambda$$

$$q \simeq \frac{2\pi}{\lambda}\varepsilon \quad 2\theta = \varepsilon$$

$$I(0) = (\rho_1 - \rho_2)^2 N v^2$$

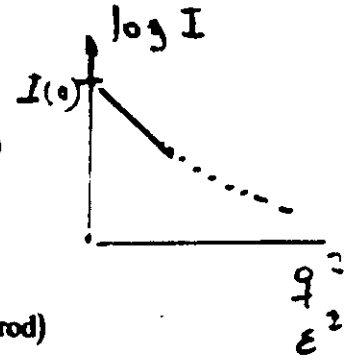

$$I(q) = I(0)\, e^{-\frac{1}{3}R_g^2 q^2} \quad \text{(Guinier)}$$

$$\lim Iq^4 = \alpha + \beta q^4 \quad (q \to \infty) \text{(Porod)}$$

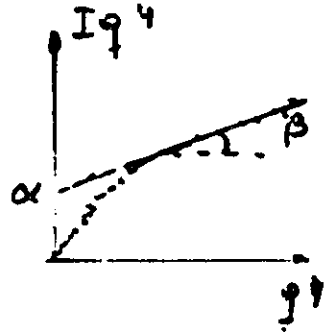

$$Q = \int_0^\infty I(q)\, q^2 dq$$

$$Q = (\rho_1 - \rho_2)^2 N v$$

Diagram of the small-angle X-ray scattering installation at L.U.R.E.

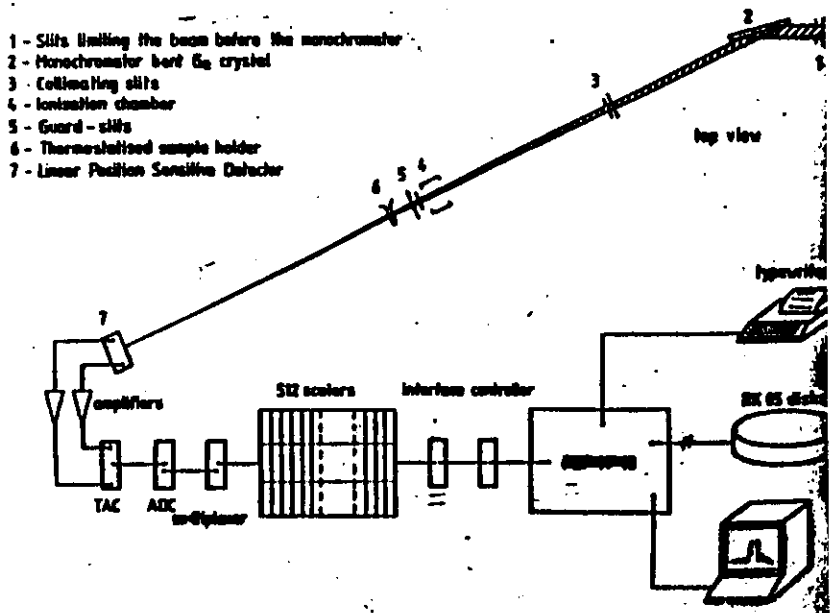

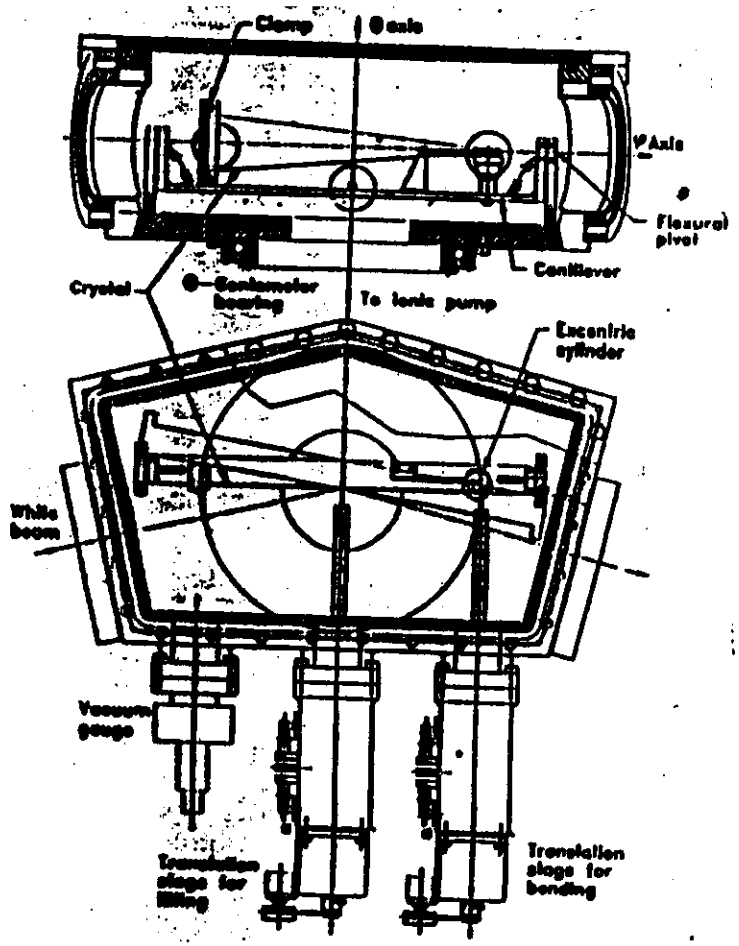

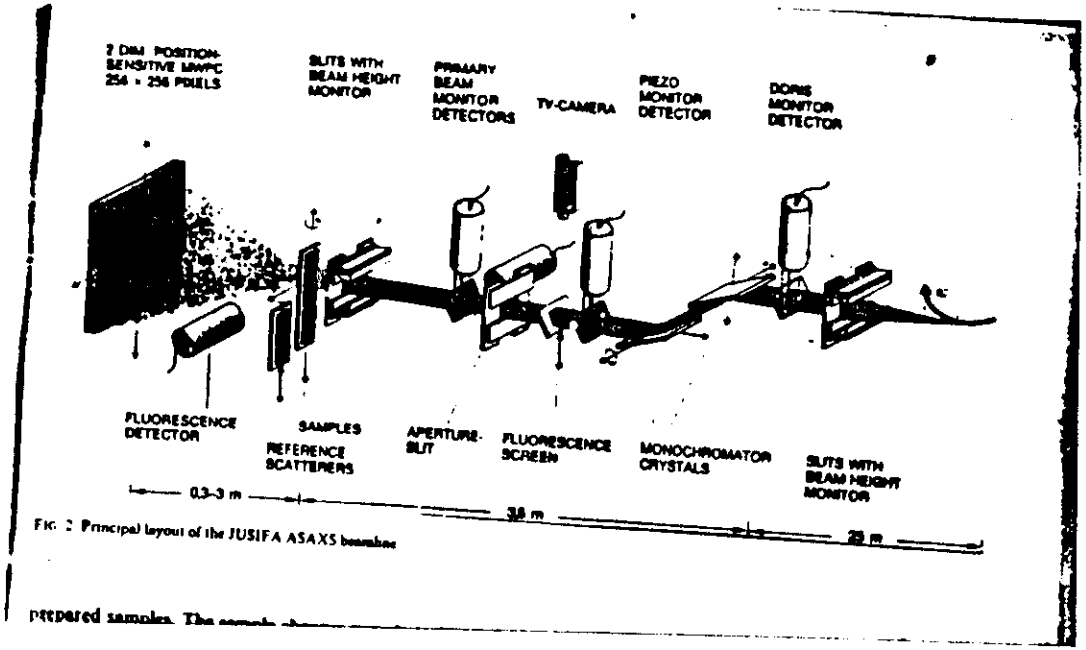

FIG. 2 Principal layout of the JUSIFA ASAXS beamline

prepared samples. The sample

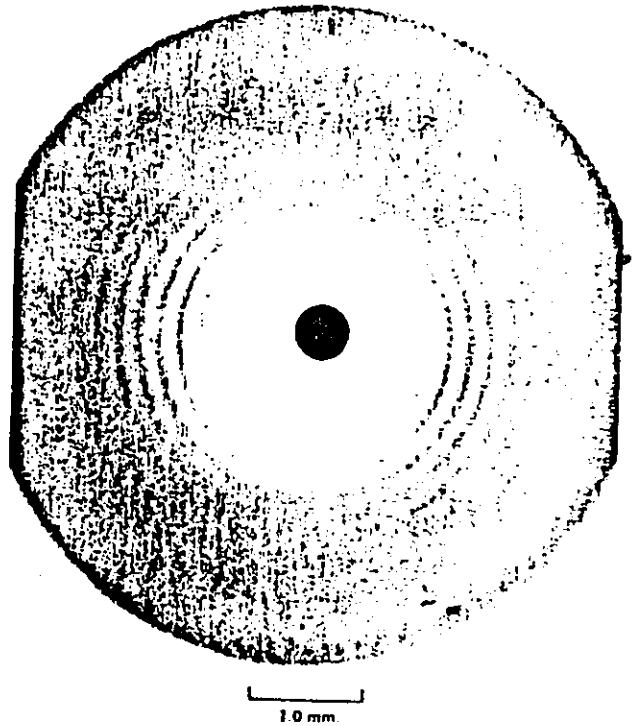

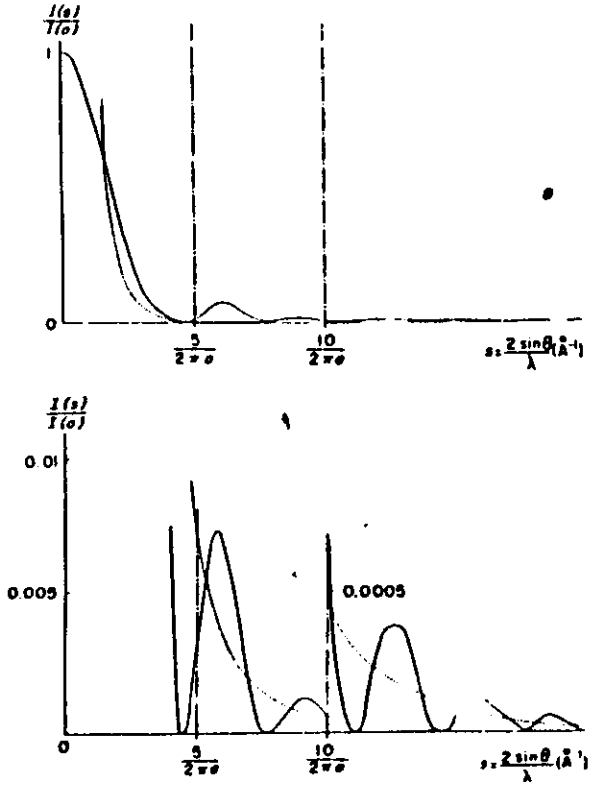

maxima clearly defined. In figure 2 these maxima seemed to be present but they could hardly be defined. A typical 100 second scan is shown in figure 3-A, where it is being compared with the average of four 200 second scans (curve B) in order to evaluate possible radiation damage to the protein.

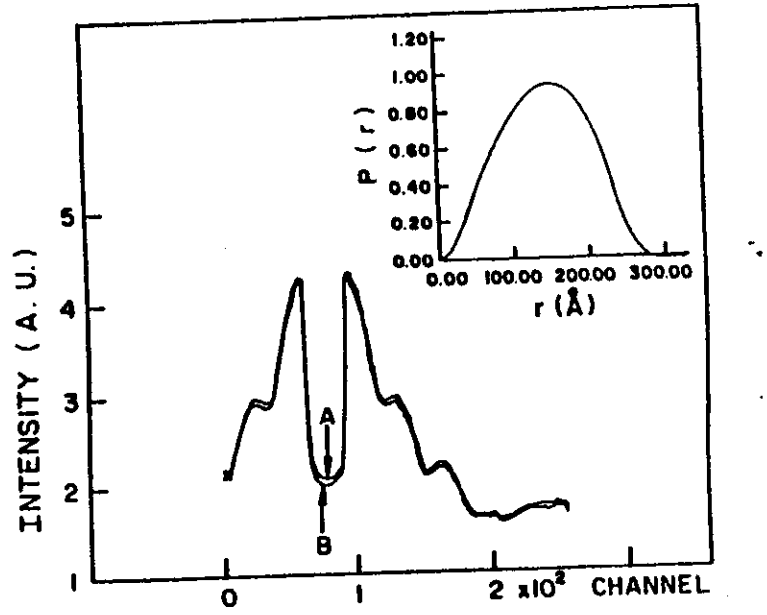

Figure 3. Experimental X-ray scattering curves from G.paulistus erythrocruorin obtained with synchrotron radiation. (A) One 100 second scan. (B) Average of four 200 second scans. The loss of intensity seems to be due to radiation damage suffered by the protein. Zero angle corresponds to channel 80, channel width = 0.000264 A^{-1}. The inset shows the distance distribution function calculated for a less concentrated sample (c/20).

Guinier plot calculations from the low concentration scattering curves (c/20 and c/40) resulted in values for the radius of giration in very good agreement with our previous calculations: 116 A. Data treatment via the inverse transformation method (ITP program) has

Glass - crystal nanocomposites

FABRICATION

Melt (1350 °C, 40 min.) < Low melting point glass - (borosilicate)

Semiconductor elements.

fast cool down

AFTER MELTING

supersaturated solid solution ⇒ glass + semiconductor elements

NO QUANTUM DOTS

Heat treatment (500 - 600 °C)

Quantum dots development

Size controlled by temperature and time.

t=0

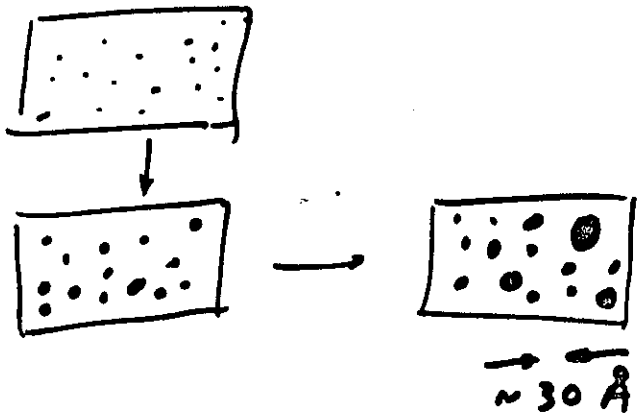

Sistema diluído de esferas com distribuição do tamanho

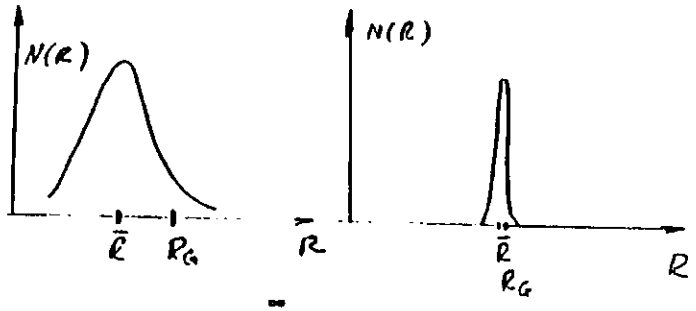

$$I(q) = \int_0^\infty N(R)\, R^6\, I_o(q,R)\, dR$$

$$\langle R^n \rangle = \int_0^\infty R^n\, N(R)\, dR$$

$$\left(\int_0^\infty N(R)\, dR = 1\right)$$

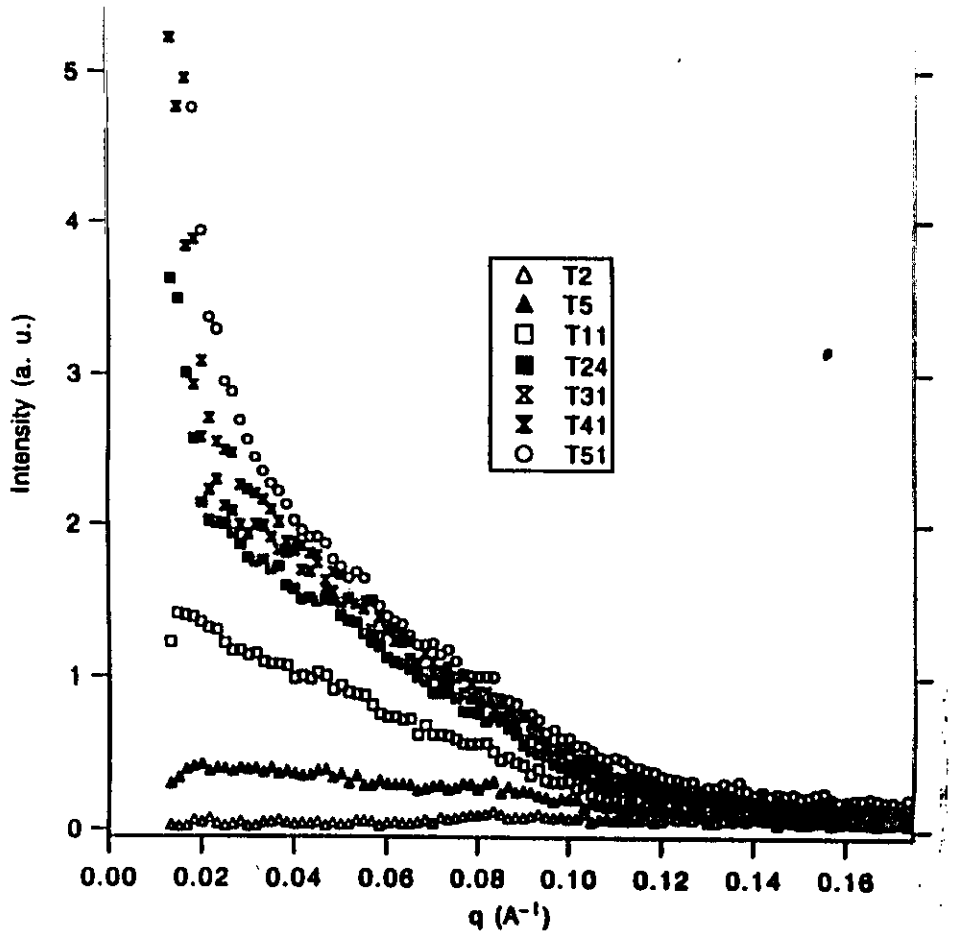

$$R_g = (5/3)^{1/2} \langle R_G \rangle = [\langle R^8 \rangle / \langle R^6 \rangle]^{1/2}$$

where $\langle R_G \rangle = 3^{1/2} \{ -\lim [d \ell n\, I(q)/d(q^2)]\ (q \to 0) \}^{1/2}$ (Guinier law)

$$R_v = (3/4\pi)^{1/3} \langle V \rangle^{1/3} = [\langle R^6 \rangle / \langle R^3 \rangle]^{1/3}$$

where $\langle V \rangle = 2\pi^2 I(0) / Q$ and $Q = \int_0^\infty q^2 I(q)\, dq$

$$R_p = (3/4) \langle D \rangle = \langle R^3 \rangle / \langle R^2 \rangle$$

where $\langle D \rangle = (4/\pi) \int_0^\infty q^2 I(q)\, dq / K$ and

$K = \lim [I(q)\, q^4\ (q \to \infty)]$ (Porod law)

$$N(R) = \frac{1}{R(2\mu)^{1/2}\, \ell n \sigma} \exp\left[-\frac{(\ell nR - \ell n\mu)^2}{2\ell n^2 \sigma} \right]$$

$$\ell n\, R_i = \ell n\, \mu + \ell n^2 \sigma\, k_i \quad ; \quad k_i\ (i = p, v, g) = R_p, R_v, R_g, \text{ respectively}$$

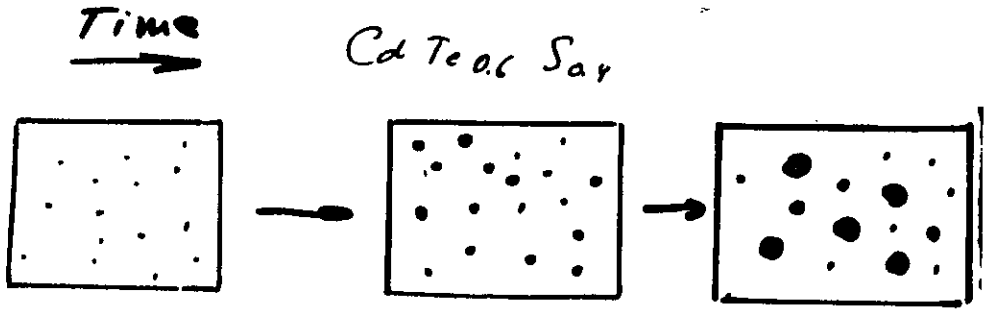

CdTe – Borosilicate glass

$$\langle d \rangle = \frac{4}{\pi} \int_0^\infty q^2\, I(q)\, dq \,/\, K_P \;; \qquad R_d = \frac{3}{4} \langle d \rangle = \langle R^3 \rangle / \langle R^2 \rangle$$

$$(K_P = \lim_{q \to \infty} I q^4)$$

$$\langle \ell \rangle = \pi \int_0^\infty q\, I(q)\, dq \,/ \int_0^\infty q^2\, I(q)\, dq \;; \qquad R_\ell = \frac{2}{3} \langle \ell \rangle = \langle R^4 \rangle / \langle R^3 \rangle$$

$$\langle I \rangle = 2\pi \int_0^\infty I(q)\, dq \,/ \int_0^\infty q^2\, I(q)\, dq \;; \qquad R_I^2 = (5/4\pi) \langle I \rangle = \langle R^5 \rangle / \langle R^3 \rangle$$

$$\langle v \rangle = 2\pi^2\, I(o) \,/ \int_0^\infty q^2\, I(q)\, dq \;; \qquad R_v^3 = (3/4\pi) \langle v \rangle = \langle R^6 \rangle / \langle R^3 \rangle$$

$$\langle R_G \rangle = 3^{1/2} \left[-\lim d\,(\ell n\, I(h)) / d(h^2) \right]^{1/2} \;; \qquad R_g^2 = (5/3) \langle R_G \rangle^2 = \langle R^8 \rangle / \langle R^6 \rangle$$

G. Walter et al. J. Appl. Cryst. 18, 205 (1985).

$$N(R) = \frac{1}{R\,(2\pi)^{1/2}\,\ell n\,\sigma}\; e^{-\frac{[(\ell n R - \ell n \mu)]^2}{2\,\ell n^2 \sigma}}$$

$\ell n\, R_i = \ell n^2\, \sigma \,.\, k + \ell n\, \mu$

k = 2,5 para l = d k = 3,5 para l = ℓ

k = 4,0 para l = I k = 4,5 para l = v

k = 7,0 para l = g

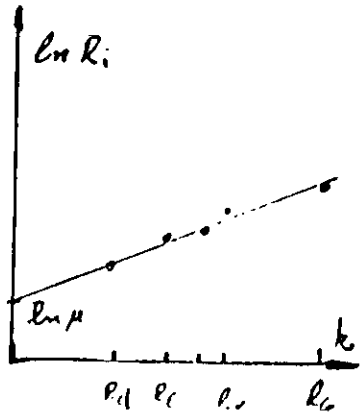

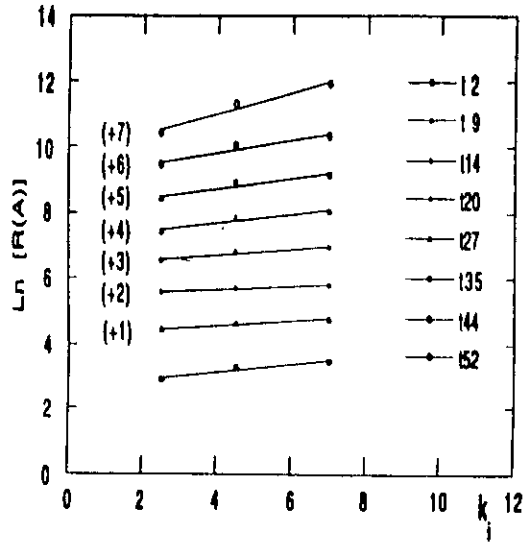

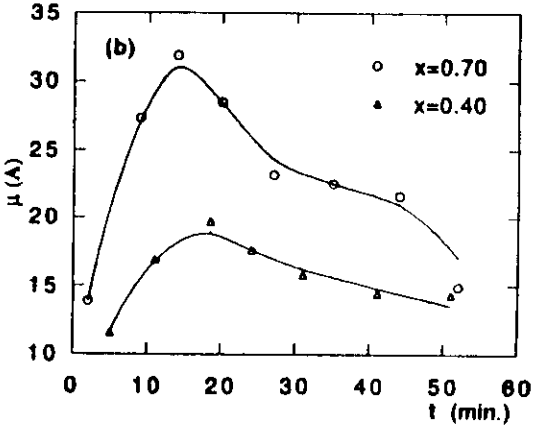

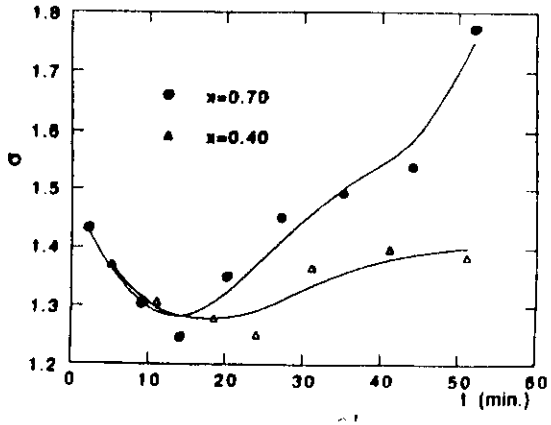

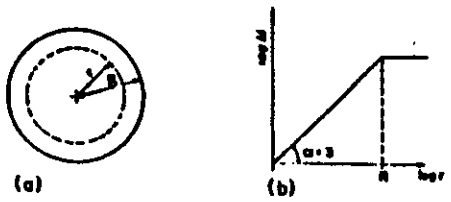

FIG. 4

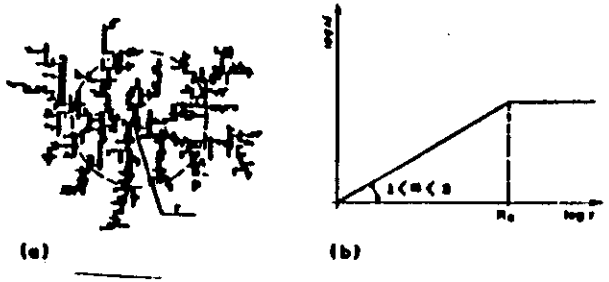

FIG. 5

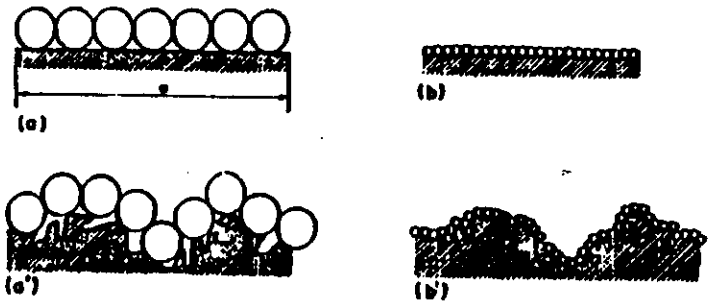

FIG. 6

$$N(r) = \phi \int g(r)\, 4\pi r^2\, dr$$

$$dN(r) = \phi\, g(1)\, 4\pi r^2\, dr$$

$$N(r) = \left(\frac{r}{r_o}\right)^D$$

$$\phi\, g(r) = (D/4\pi r_o)\, r^{D-3}$$

$$\phi\, g(r) = (D/4\pi r_o)\, r^{D-3} \cdot e^{-\frac{r}{\xi}}$$

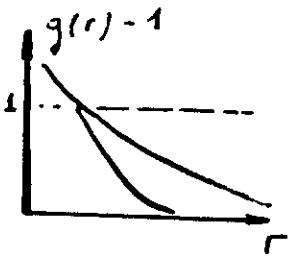

The introduction of the out-off function $e^{-\frac{r}{\xi}}$ avoids the divergence in the calculation of: $S(q)$

$$S(q) = 1 + 4\pi\phi \int [g(r) - 1]\, r^2\, \frac{\operatorname{sen} qr}{qr}\, dr$$

The calculation of S (q) leads to:

$$S(q) = 1 + \frac{1}{(q r_0)^D} \frac{D\,\Gamma(D-1)}{\left[1 + 1/(q^2 \xi^2)\right]^{(D-1)/2}} \times \sin\left[(D-1)\,\mathrm{tg}^{-1}(q\xi)\right]$$

$q \ll \xi^{-1}$ ⇓ $- P(D-1)(\xi / r_0)^D \times \left[1 - [D(D+1)/6] Q^2 \xi^2\right]$

$\xi^{-1} \ll q \ll r_0^{-1}$ ⇓ $\propto q^{-D}$

$q \gg r_0^{-1}$ ⇓ $\propto q^{-4}$ or $\propto q^{-(6 - D_S)}$

$I(q) = I(0)\, e^{-\frac{1}{3} R^2 q^2}$

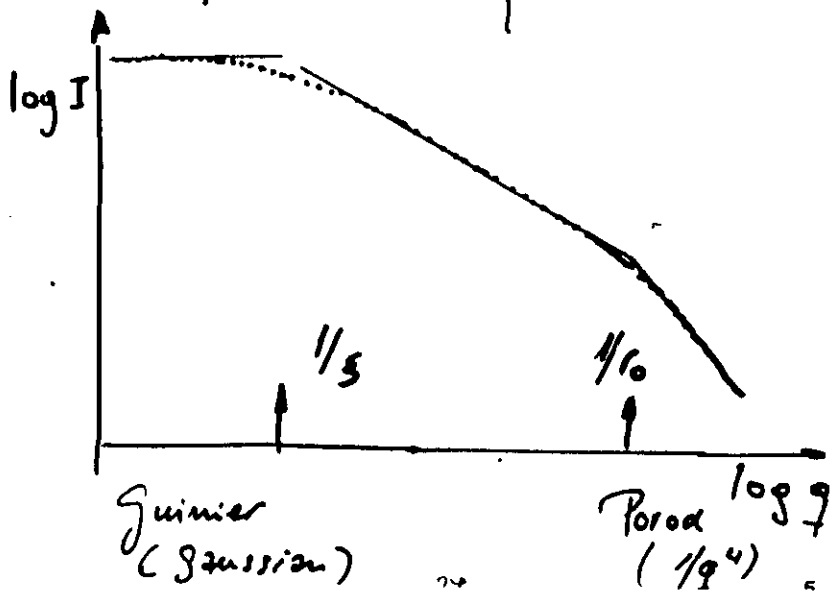

2.I

$\propto e^{-\frac{1}{3} R_G^2 q^2}$

$\propto \begin{cases} 1/q^{D_v} \\ 1/q^{(6-D_S)} \end{cases}$

$\propto 1/q^4$

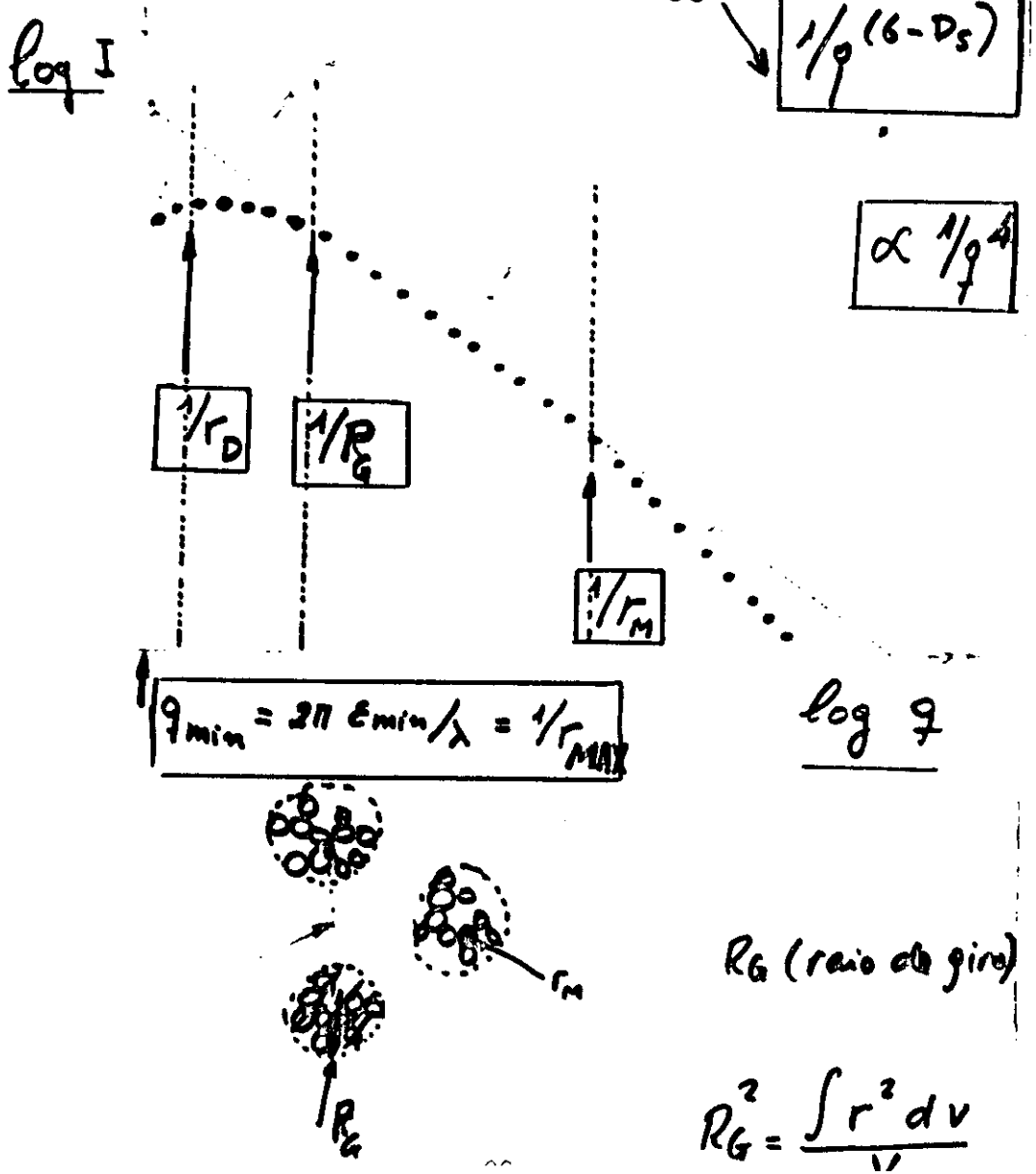

R_G (raio de giro)

$R_G^2 = \frac{\int r^2 dv}{V}$

STRUCTURAL STUDY OF FRACTAL SILICA HUMID GELS

A. CRAIEVICH

Laboratório Nacional de Luz Sincrotron, CNPq, Campinas, and Instituto de Física, Universidade de São Paulo, São Paulo, Brazil

D.I. dos SANTOS and M. AEGERTER

Instituto de Física e Química de São Carlos, Universidade de São Paulo, São Carlos, SP, Brazil

F. LOURS and J. ZARZYCKI

Laboratoire de Science des Matériaux Vitreux, Université du Languedoc, Montpellier, France

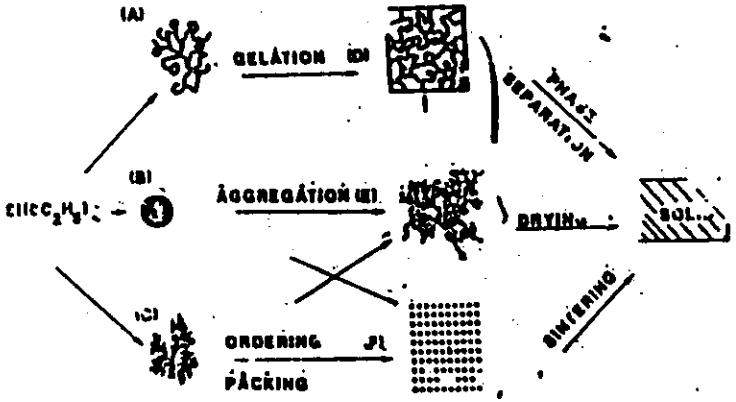

Fig. 1 Precursors to glass and ceramic materials

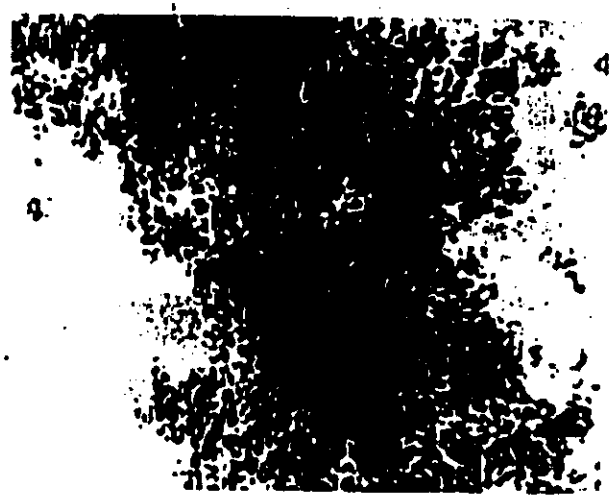

FIGURE 2
TEM microphotography of aerogel prepared from acidic sol.

UF

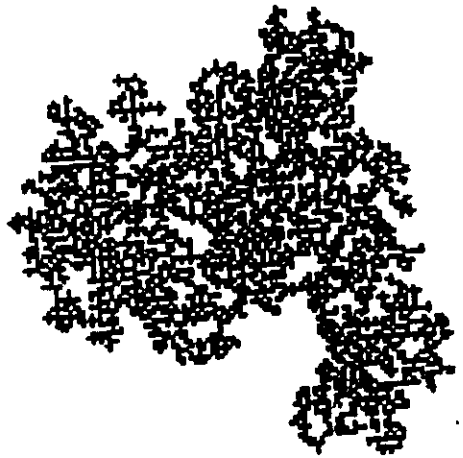

(2H+3H+FH) M

D = 1.8 F

3H M

D = 2 NF

A. Craievich, D. Chaumont, J. Zarzycki
LNLS, Brazil Univ. Montpellier

Aggregation kinetics and structure of precursor gels of zirconia under different preparation conditions

Introduction

Motivation

SAXS results

Conclusions

Sol-gel route to glasses

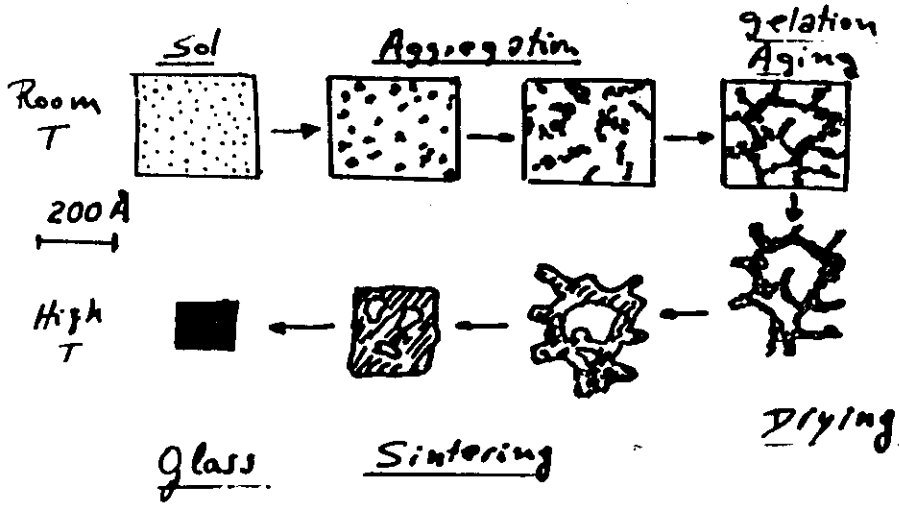

— TMOS + Methanol + water

- TEOS + Ethanol + water

TMOS + water + ultrasound

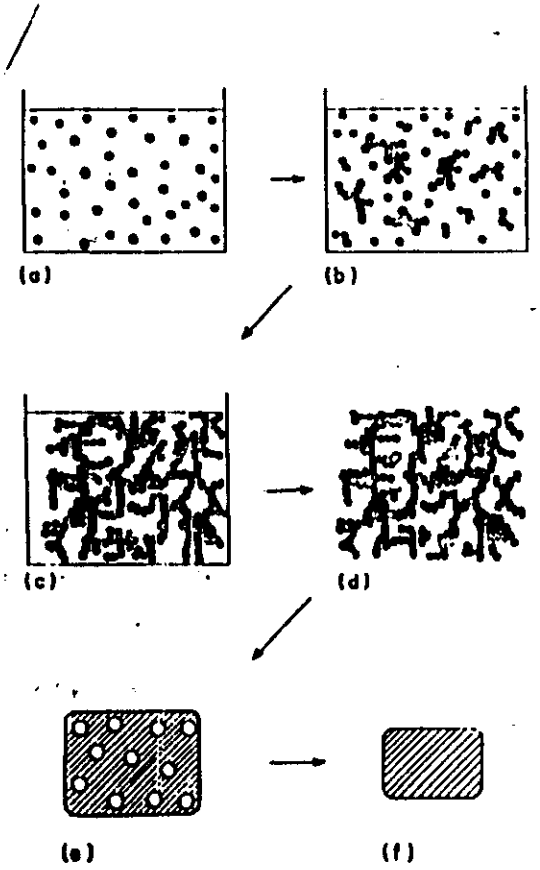

FIG. 11

TMOS + Metanol (Meio básico)

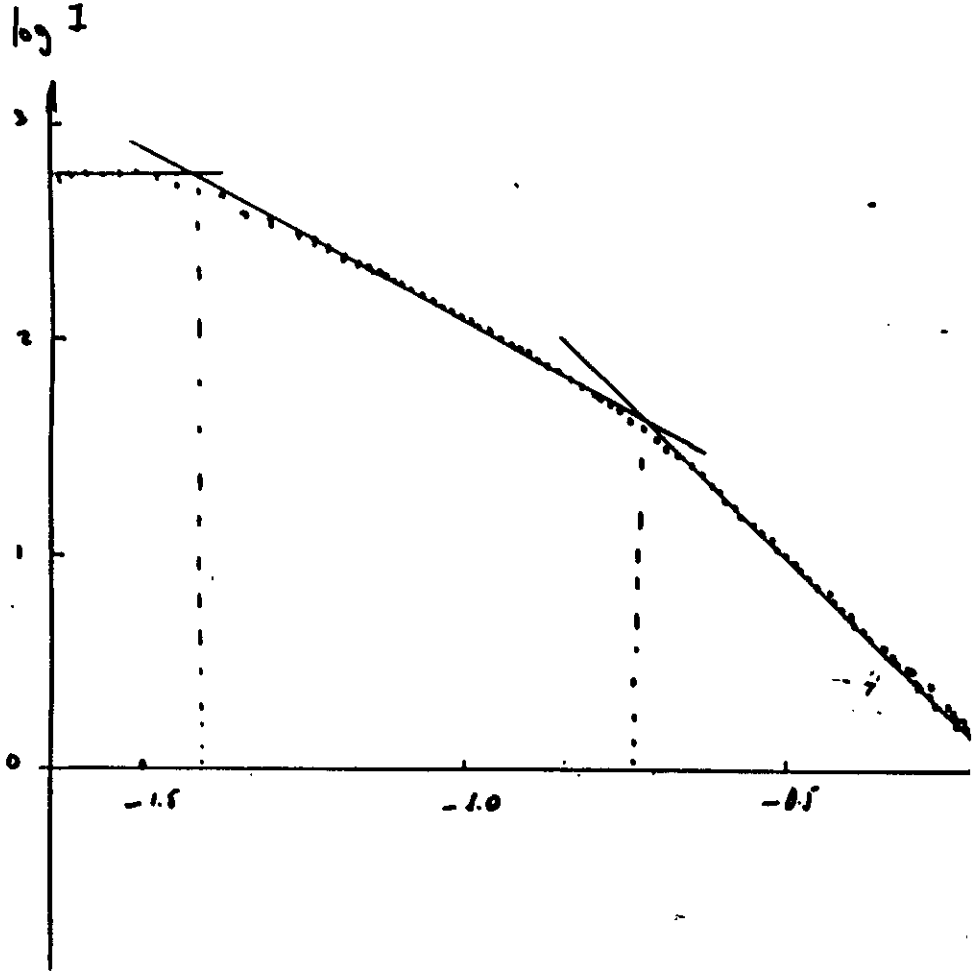

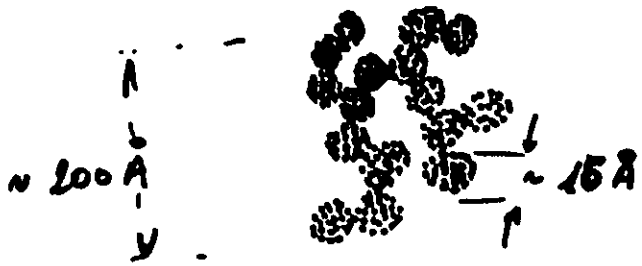

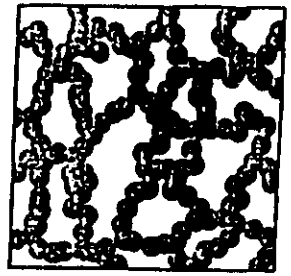

FIG. 2. Schematic diagram of the structure suggested for silica aerogel.

A : silica aerogel
B : agregate of silica particles
C : colloidal monomer

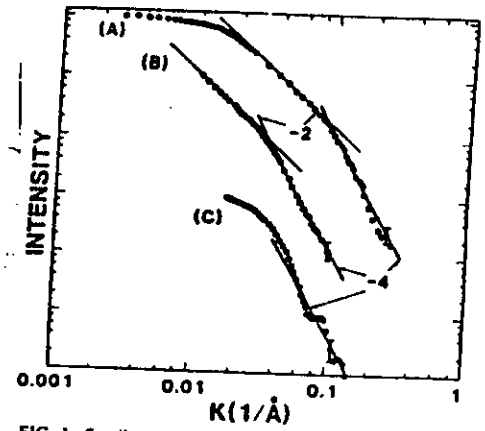

FIG. 1. Small-angle x-ray scattering curves for (curve A) silica aerogel ($\rho = 0.088$ g/cm^3), (curve B) a solution aggregate of silica particles (Ref. 12), and (curve C) the colloidal monomer. No crossover to K independence at small K is observed for the aggregate because of the large size ($> 1\ \mu$m). The similarity of curves A and B indicates that the aerogel and the aggregate are structurally similar. More extensive light scattering data (Ref. 13) show a slope of -2.1 for the aggregate in the regime $K < 0.01$ Å^{-1}.

Chaumont, Craievich, Zarzycki
J. Non Cryst. Solids 1992

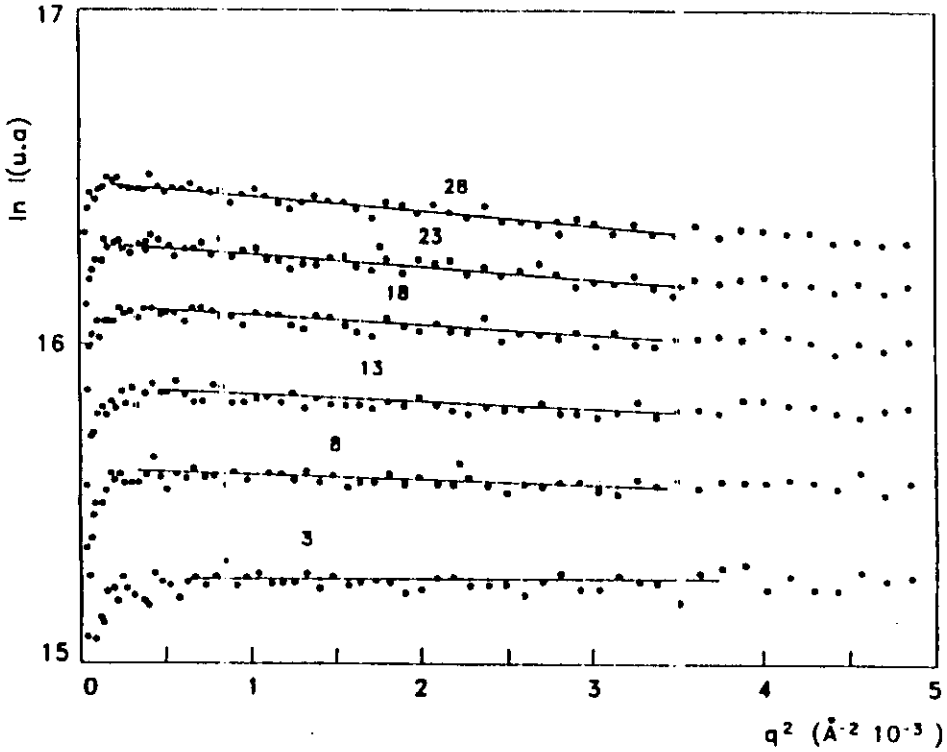

Fig. 1a: Guinier's plots corresponding to a sample solution 10 $Zr(O\,Pr)_4$ - 3 acetic acid without ultrasound for the indicated aggregation times (min.) a 60 °C (early stages of aggregation).

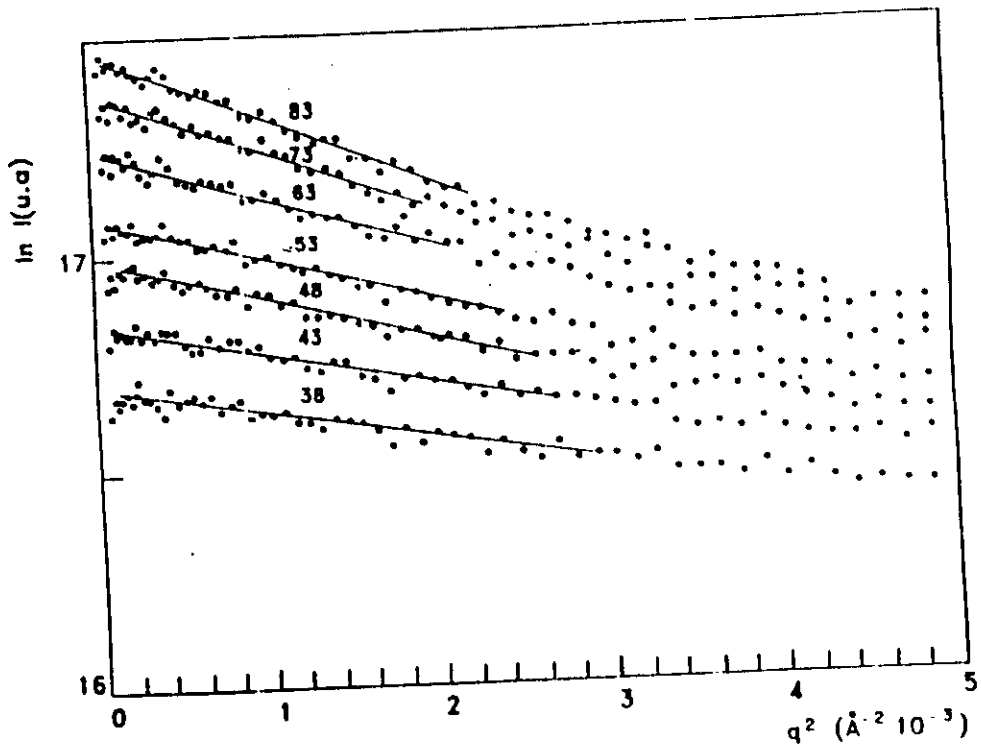

Fig. 1b: Guinier's plots corresponding to the same composition than in Fig. 1a for advanced stages of aggregation and gelation, as functions of the indicated aggregation times (min.).

Silica - TMOS sol

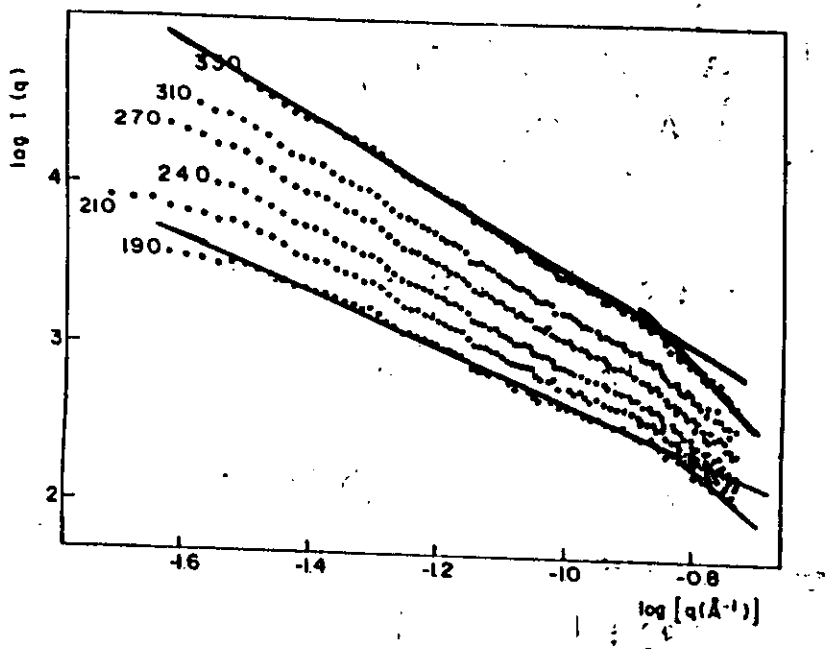

FIG. 1

2.1 Isothermal spinodal decomposition

$$\frac{\partial c(\vec{r},t)}{\partial t} = D\nabla^2 c(\vec{r},t) - \kappa'\nabla^4 c(\vec{r},t) \qquad (1)$$

$$I(k,t) = I(k,0)\, e^{2R(k)t} \qquad (2)$$

$$R(k) = -Dk^2\left(1-\frac{k^2}{k_C^2}\right) \qquad k_M = k_C/\sqrt{2}. \qquad (3)$$

$$I(k,t) = |\, I(k,0) - L(k,T_E)\,|\, e^{2R(k)t} + L(k,T_E) \qquad (4)$$

$$D(t) = D + D' e^{-\frac{t}{\tau}} \qquad (5)$$

$$I(k,t) = I(k,0)\, e^{2R(k)t}\, e^{2R'(k)\tau\left(1-e^{-\frac{t}{\tau}}\right)} \qquad (6)$$

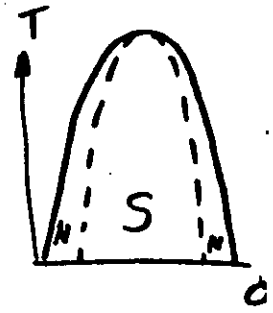

2.2 Nucleation and Growth

$$R = \gamma/Dt \qquad (7)$$

$$I(k) = A R^6 e^{-\frac{1}{5}R^2k^2} \qquad (8)$$

$$A(k_i,t) = A' t^3 e^{-\frac{1}{5}\gamma' k_i^2 t} \qquad (9)$$

2.3 Coarsening

$$A(t) = \int k^2 I(k,t)\,dk \qquad (11)$$

$$\bar{R}^3 = \alpha + \beta t \qquad (10)$$

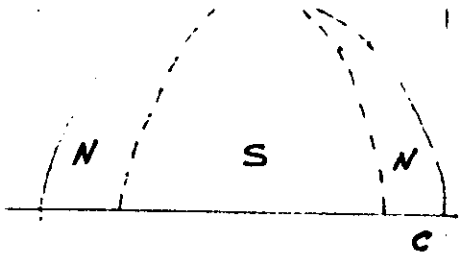

Phys. Rev. B
15, 15 (1977)

KINETICAL ISING MODEL

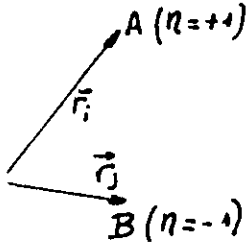

$$U = -J \sum \eta(\vec{r}_i).\eta(\vec{r}_j) \qquad J > 0$$

$$P_{ij} = \propto e^{-\beta \Delta U_{ij}}/(1+e^{-\beta \Delta U_{ij}})$$

$$\beta = 1/k_B T \qquad \propto = \gamma_0 e^{-\phi/k_B T}$$

$$4\ J/T_c\ k_B = 0.89$$

— $S(\vec{q},t) = \sum_{\vec{r}} e^{i\vec{q}.\vec{r}} \sum_i [\eta(\vec{r}_i,t) - \bar{\eta}][\eta(\vec{r}_i+\vec{r},t)-\bar{\eta}]$

— $S(\vec{q},t) = I(\vec{q},t)$

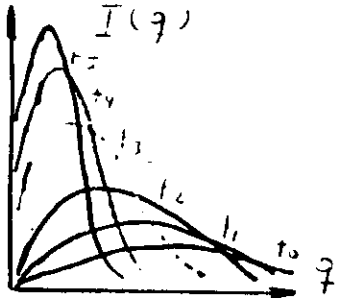

SCALING PROPERTIES OF THE STRUCTURE FUNCTION

— $S_n(t) = \int q^n I(q,t)\, dq$

— $q_n(t) = S_n/S_0$

— $\underline{S(q,t).\ q_1^3(t)}$
or
— $\underline{I(q,t).\ q_1^3(t)}$

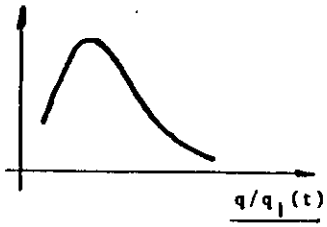

$q_1 \propto t^{-a}$

$a \simeq 0.22$

$a \simeq 0.29$

Marro et al.
Phys. Rev. Lett.
43, 282 (1979)

Dynamical scaling:

$$S(q,t) = [K(t)]^{-3}\, F[q / K(t)]$$

$$K(t) = q_1(t)$$

$$q_1(t) = \frac{\int q\, S(q,t)\, dq}{\int S(q,t)\, dq}$$

1) $q_1 \propto t^{-a}$

2) $S_M \propto t^{+a'}$

$$a' = 3a$$

3) $q_2 \propto q_1^2 \therefore \frac{q_2}{q_1^2} \neq f(t)$

4) $F(q/q_1) = q_1^3\, S\left(q/q_1, t\right)$

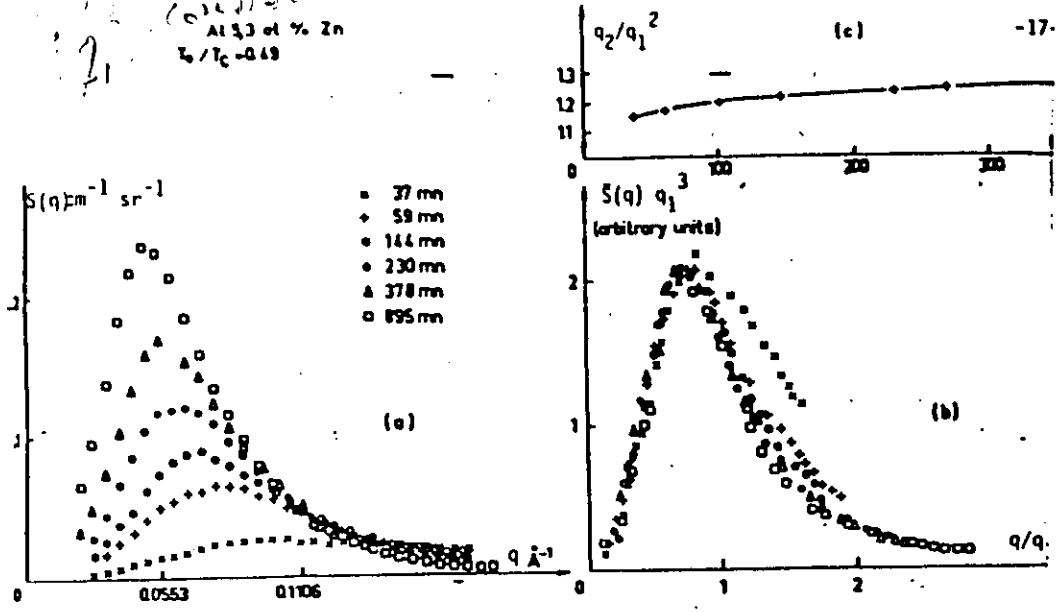

Fig. 12 : Al-5,3 at.% Zn. T = 20°C. a) S(q,t) moyen pour différents temps de vieillissement. b) $\bar{S}(q).q_1^3 = f(q/q_1)$. c) q_2/q_1^2.

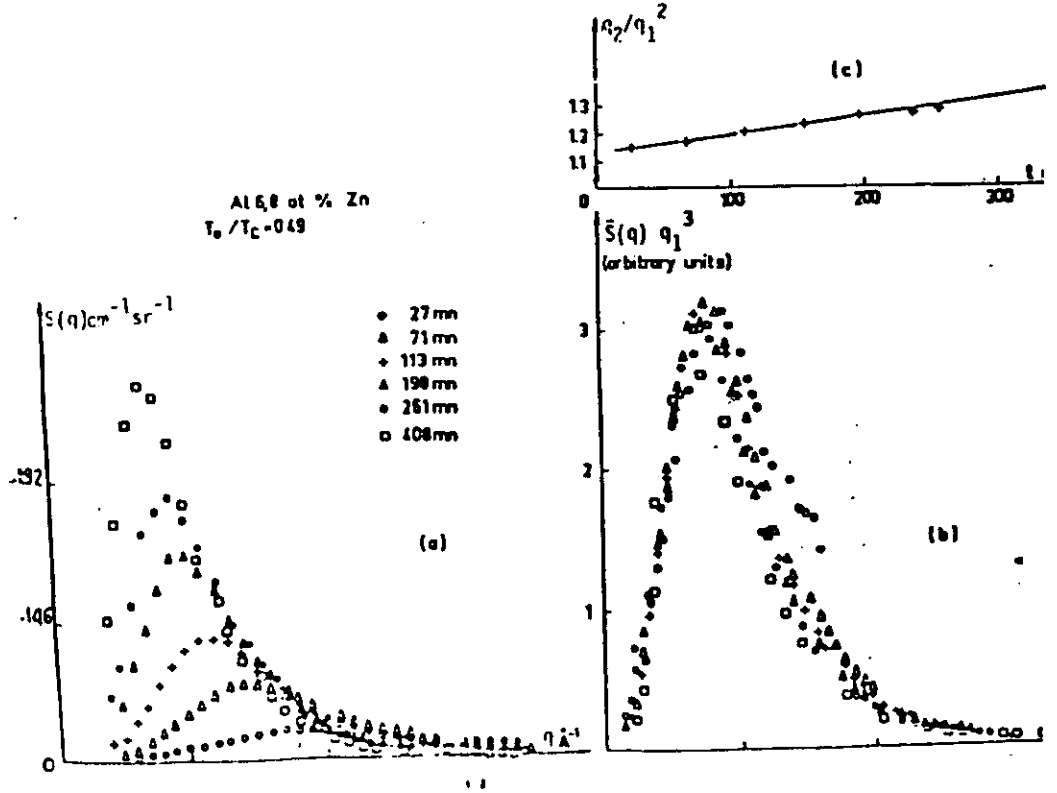

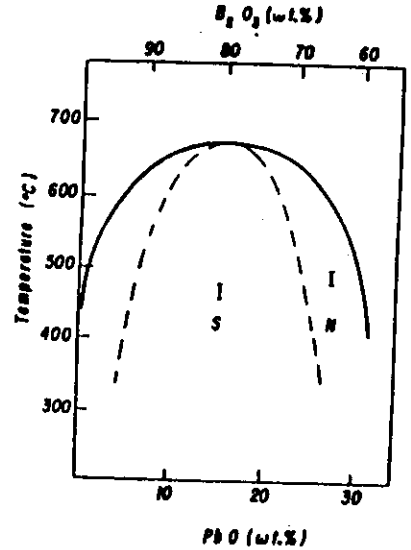

FIG. 1. Miscibility gap for the quasibinary B_2O_3-PbO-Al_2O_3 glass system, from Ref. 15. The continuous line corresponds to the solubility limit and the dashed line is the classical spinodal. The bars *S* and *N* indicate the composition and temperature range investigated in this work.

Crizewich
Sanchez
Williams
Phys Rev. B
34, 2762 (1986)

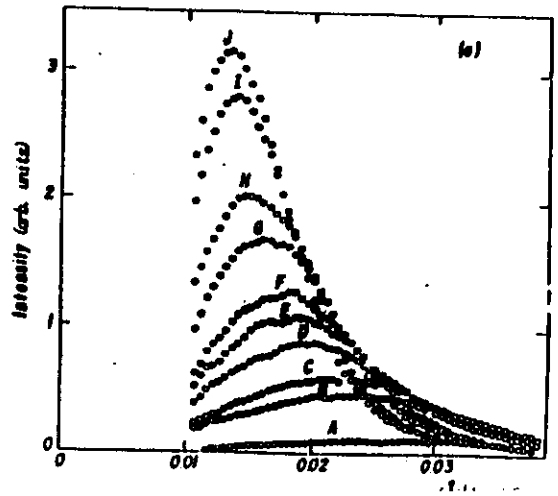

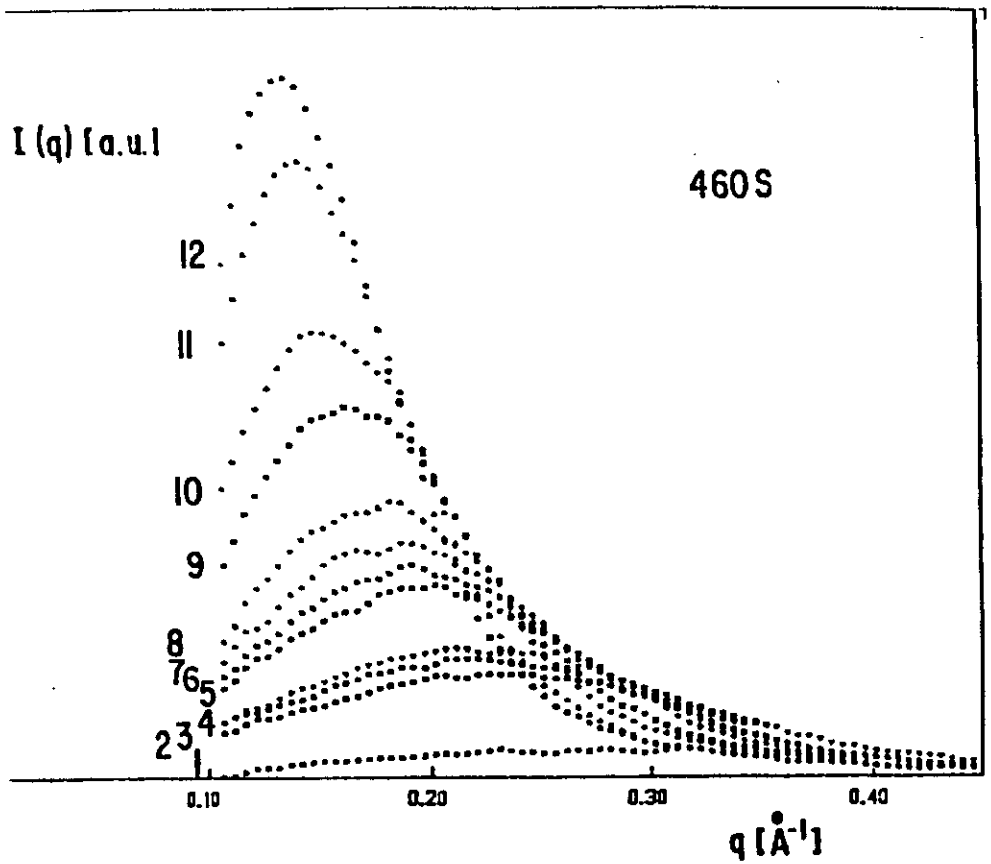
I (q) [a.u.]
460 S
12
11
10
9
8
7
6
5
4
3
2
1
0.10
0.20
0.30
0.40
q [Å⁻¹]

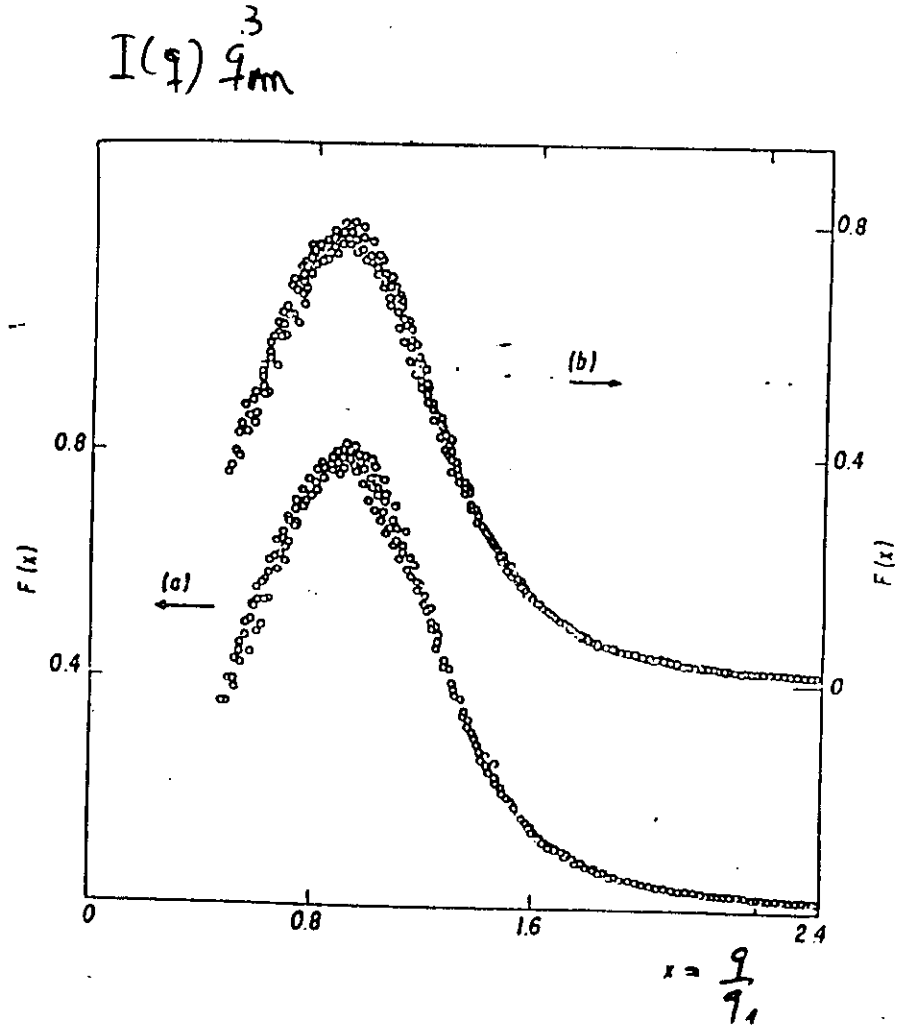
I(q) q_m^3
(b)
(a)
F (x)
F (x)
0.8
0.4
0
0.8
0.4
0
0.8
1.6
2.4
x = q/q_1

Fig. 8

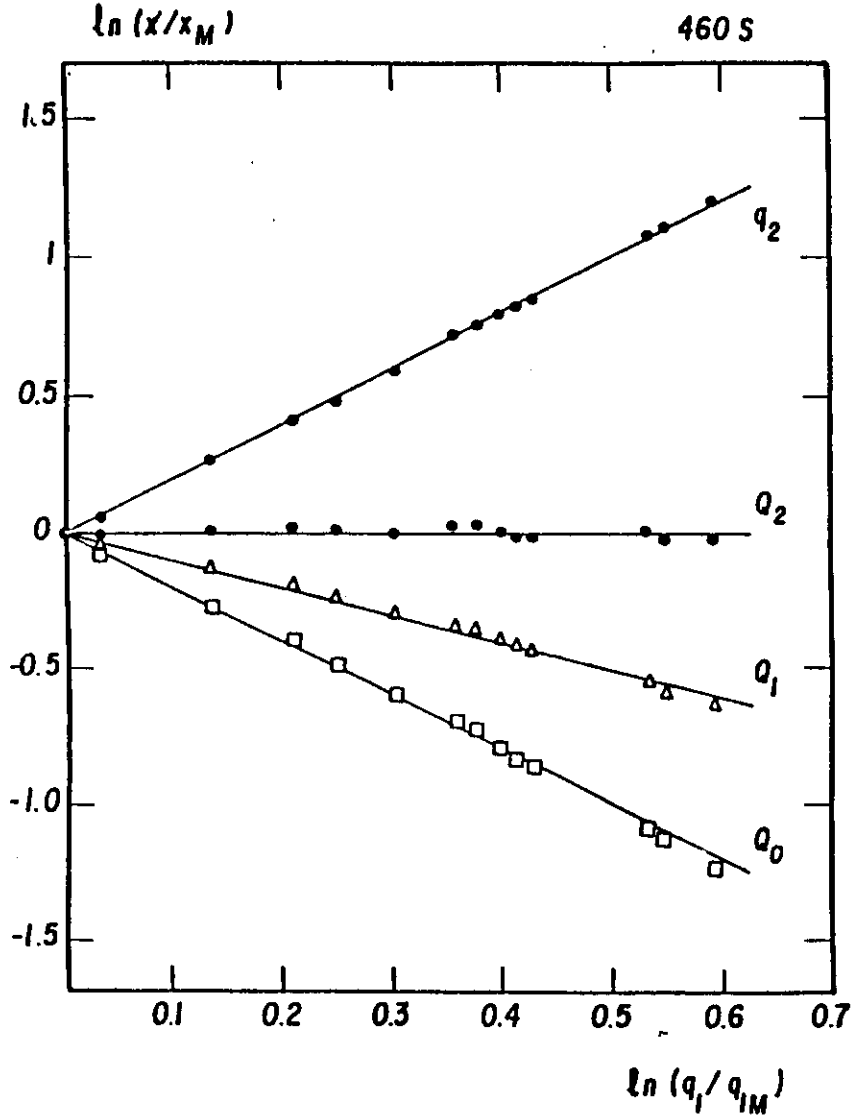
ln (x/x_M)
460 S
1.5
1
0.5
0
-0.5
-1.0
-1.5
0.1
0.2
0.3
0.4
0.5
0.6
0.7
q_2
Q_2
Q_1
Q_0
ln (q_1/q_1M)

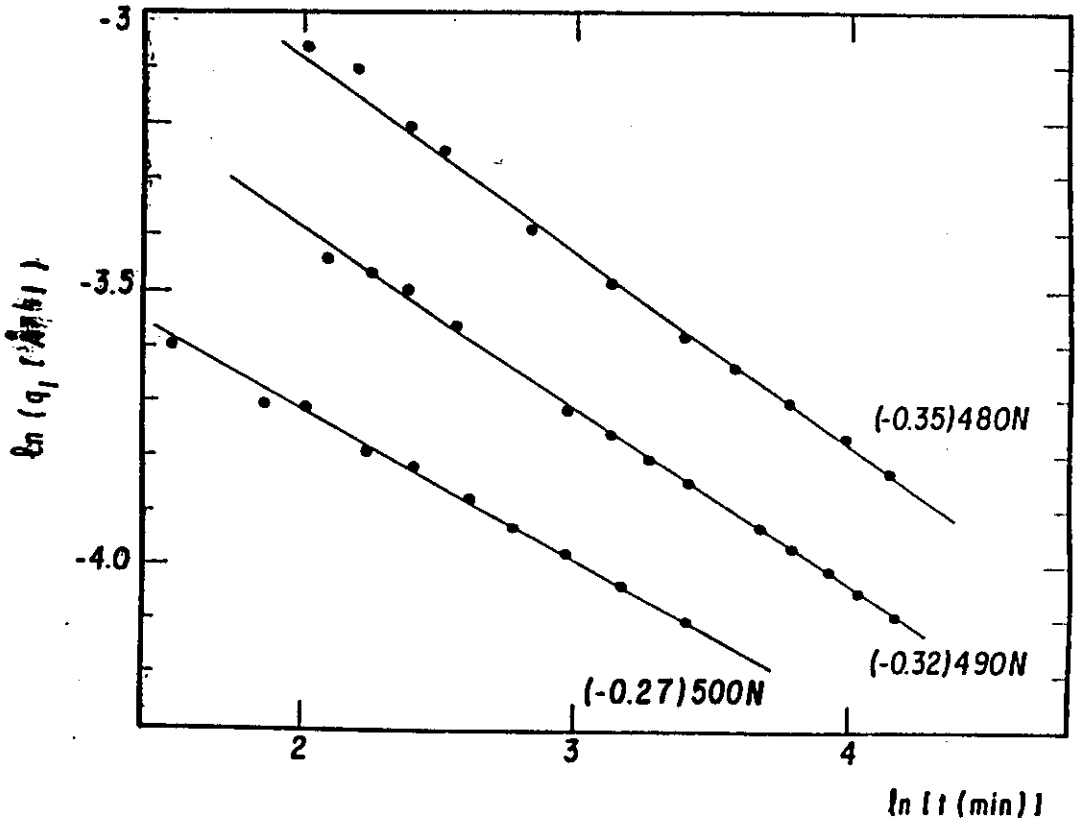
-3
-3.5
-4.0
2
3
4
(-0.35)480N
(-0.32)490N
(-0.27)500N
ln [t (min)]

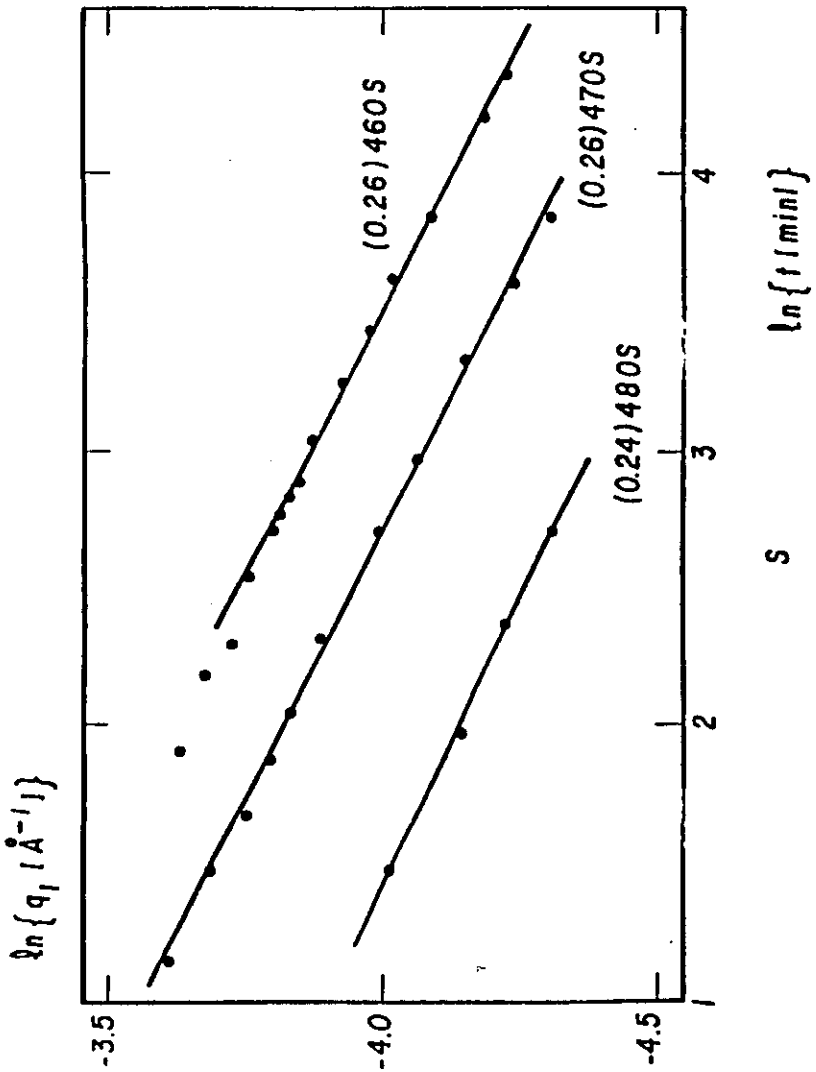

SPINODAL REGION

- Theory of spinodal decomposition (Cahn) Linear theory (valid only for early stages).
- Reasonable agreement with experiments on alloys (Al-Zn, Au-Pt).
- Poor agreement with experiments on glasses (B_2O_3-PbO-Al_2O_3, SiO_2-Na_2O).

NUCLEATION AND GROWTH

- Classical diffusion theory ("GP" zones in alloys and "droplets" in glasses).
- Ambiguous comparisons between theory and experiments.

NEW THEORIES

- Kinetical Ising model for simple cubic lattice.
- Calculations by computer simulation using Monte Carlo method.
- Scaling properties and "universality".

Cahn's theory was applied to explain the kinetics of SAXS from real phase separation systems under isothermal conditions and, we could say, that it has had an only limited sucess for early stages in alloys.

Its agreement with experimental results in glassy systems was poorer, probably because of the intrinsic impossibility for isolators of reaching high quanching rates.

Recent new theoretical developments have considerably simplified the picture of phase separation. They are based on the Ising model for ferromagnets applied to binary alloys by using computer simulation and the Monte Carlo method.

This theories lead to scaling and "universality" properties of the structure function.

The first theoretical study of the complex phenomena of phase separation in solids was provided by the now classic theory of spinodal decomposition of Cahn. Central to the theory is the fact that, within the "spinodal" region, the homogeneous mixture is unstable to small concentration fluctuations of the system. The evolution equation of the Fourier components of the atomic composition and, consequently, of the small angle X-ray scattering intensity could only be solved in closed form after linearization. Therefore it can only be applied to very early stages of phase separation.

Outside of the spinodal region, i.e. near the boundary of the miscibility gap, the decomposition process was described by the classical diffusion theories of nucleation and growth of "GP zones" (in alloys) or "droplets" (in glasses).

CONCLUSIONS

- Real space analysis (T.E.M.) does not allow quantitative studies of phase separation.

- Cahn theory for spinodal decomposition is not a good approximation for isothermically phase separating real glasses.

- The statistical dynamic Ising model describes well the advanced stages of phase separation in glasses.

- Some discrepancies related to the scaled structure function have been detected in the B_2O_3-PbO-Al_2O_3 system.

ASAXS

The scattered intensity may be written as

$$I(q) = \Sigma\ \Sigma f_j\ f_k^*\ S_{jk}\ (q)$$

$S_{jk} = S_{kj}^*$ is the partial structure factor

$$f_j = f_j^o + f_j^{'}(E) + i f_j^{''}(E)$$

$$f_j^o(q \to 0) = Z_j$$

The ASAXS allows for the determination of the partial structure function S_{jk}.

Binaire systems (1,2)

$$I(E,q) = F_1(q,E)^2 S_{11} + 2F_1(E) F_2(E) \cos\varphi S_{12} + F_2(E)^2 S_{22}$$

In order to obtain S_{11}, S_{12} and S_{22} it is necessary to perform three experiment at three different energies: (I, F e S are function of q).

$$I(E_1) = F_1(E_1)^2 S_{11} + 2F_1(E_1) F_2(E_1) \cos\varphi S_{12} + F_2(E_1)^2 S_{22}$$

$$I(E_2) = F_1(E_2)^2 S_{11} + 2F_1(E_2) F_2(E_2) \cos\varphi S_{12} + F_2(E_2)^2 S_{22}$$

$$I(E_3) = F_1(E_3)^2 S_{11} + 2F_1(E_3) F_2(E_3) \cos\varphi S_{12} + F_3(E_3)^2 S_{22}$$

In matricial form:

$$(\bar{I}) = (\bar{F})\,(\bar{S})$$

A method to estimate the errors propagation in solving this equation uses the Turing relation:

$$\frac{\| \Delta S \|}{\| S \|} \leq \| F \| \; \| F^{-1} \| \frac{\| \Delta I \|}{\| I \|}$$

where || A || are the norm of vectors and matrix:

$$\| A \| = (\sum_{ij} a_{ij})^{\frac{1}{2}}$$